Divergent Mechanisms of Gefitinib Hepatotoxicity in Metabolically and Genetically Diverse Hepatocyte Models

Masarone, Sara Katie V. Beckwith Philip S. Lewis Kate Cameron Hosseini-Gerami, Layla
sara.masarone@ignotalabs.ai katie.beckwith@ignotalabs.ai philip@cytochroma.org kate@cytochroma.org
layla.gerami@ignotalabs.ai

Ignota Labs
July 2026

Abstract

This white paper reports early findings from the Ignota Labs project *Understanding and Mitigating Drug Toxicity Risks in Diverse Populations through AI-Enabled Genomics and Pharmacogenomics*. Building on our previous work, in which the causal and explainable AI platform SAFEPATH predicted and experimentally validated a novel PRKD1/PRKD3-sphingolipid mechanism of gefitinib hepatotoxicity, we asked why the clinical toxicity response to gefitinib is so heterogeneous between patients. Pharmacogenomic analysis of a non-small-cell lung cancer cohort identified CYP3A4 activity as a candidate modifier, and we therefore profiled two donor-diverse, female iPSC-derived hepatocyte lines with contrasting CYP3A4 activity - i18F (low activity, predominantly Native American ancestry) and i30F (high activity, predominantly European ancestry) across five gefitinib concentrations by RNA-seq. Both lines converge on suppression of globo sphingolipid metabolism, independently reproducing the mechanism identified in our earlier case study. Beyond that shared core, the two lines diverge sharply: i18F shows early stress signalling, collapse of phase I/II biotransformation and loss of hepatocyte identity transcription factors, consistent with parent-compound accumulation; i30F mounts a high-output metabolic response with strong NRF2-ARE, oxidative stress, p53 and genotoxicity enrichment, consistent with a burden of reactive metabolites. The NRF2 signature in the higher-European-ancestry line aligns with population-level genomics, in which KEAP1-NRF2 alterations are far more frequent in Western than in East Asian NSCLC cohorts, offering a mechanistic rationale for population-specific differences in gefitinib toxicity and resistance. These findings are hypothesis-generating and define a set of specific experimental validations.

1 Introduction

Gefitinib (Iressa) is an oral targeted therapy for epidermal growth factor receptor (EGFR)-positive non-small-cell lung cancer (NSCLC) and was the first selective inhibitor of the EGFR tyrosine kinase (TK) domain. EGFR is over-expressed in several carcinomas, and point mutations in the TK domain activate anti-apoptotic signalling, disabling the normal mechanisms by which such malignancies would be eliminated. The clinical success of gefitinib led directly to the approval of further EGFR inhibitors, including erlotinib, afatinib, dacomitinib and osimertinib.

Gefitinib is nonetheless classified by the FDA as a "Most-DILI-Concern" compound [1, 2]. A substantial proportion of treated patients develop drug-induced liver injury (DILI), requiring frequent monitoring, dose interruption or a switch of agent [3]. Analysis of the FDA Adverse Event Reporting System (FAERS) shows hepatic function abnormalities as one of the most commonly reported reaction groups for gefitinib, with adverse event reports distributed unevenly across sexes (Figure 1) [4].

Figure 1: Gefitinib adverse event case counts by sex, extracted from the FAERS database. Female cases (4,706) exceed male cases (3,286); 880 reports do not specify sex.

In our previous case study [5] we applied SAFEPATH, our causal and explainable AI platform, to erlotinib and gefitinib. The known UGT1A1-mediated mechanism of erlotinib hepatotoxicity was recovered, and a previously unknown mechanism for gefitinib was predicted: inhibition of protein kinase D1 and D3 (PRKD1/PRKD3), enzymes involved in sphingolipid metabolism, whose disruption is linked to hepatocellular death and liver injury [6]. The prediction, made by CELLSCAPE from chemical structure alone, was subsequently confirmed by radiometric kinase assay (PRKD1 inhibition at 3 µM, close to the clinical maximum plasma concentration) and by transcriptomic enrichment of sphingolipid metabolism in gefitinib-treated primary rat hepatocytes. The output of that analysis is reproduced in Figure 2.

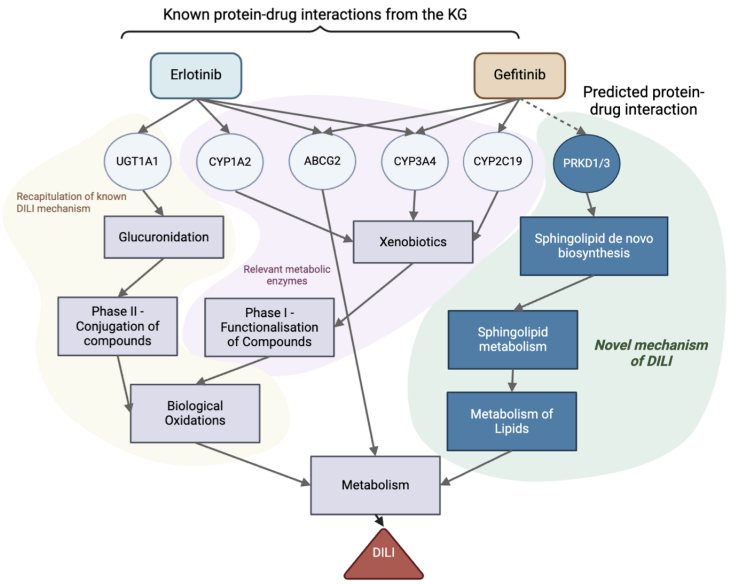

Figure 2: Output of SAFEPATH from our previous case study [5], showing recapitulation of the known erlotinib UGT1A1 mechanism (left), relevant metabolic enzymes (centre) and the novel PRKD1/3-sphingolipid mechanism of gefitinib DILI (right). Reproduced from Hosseini-Gerami et al. (2024).

That study left one clinically important question open: gefitinib hepatotoxicity is markedly heterogeneous between patients, and a single off-target mechanism does not explain why. The present work addresses that question directly. We hypothesised (i) that hepatocytes with different cytochrome P450 capacities would metabolise gefitinib differently and therefore experience different intracellular ratios of parent compound to metabolite, and (ii) that sphingolipid metabolism, downstream of PRKD1 inhibition, would remain a

component of the toxic response in both cases. To test this we combined pharmacogenomic cohort analysis, phenotypic screening of a donor-diverse iPSC-derived hepatocyte panel, concentration-resolved RNA-seq, footprint-based pathway and transcription factor inference, and structure-based target prediction for gefitinib metabolites.

2 Methodology

2.1 Cohort selection and pharmacogenomic variant analysis

The number of gefitinib-treated patients with linked genomic data was insufficient for statistical analysis. We therefore assembled a cohort of NSCLC patients irrespective of treatment from Genomics England (GEL). The cohort is predominantly of white British, other European and American/Native American ancestry, with an approximately equal distribution of sexes. Small variant analysis (SVA) was performed across the cohort to identify common germline variants, and the resulting variant set was cross-referenced against PharmGKB [7] to retain variants with documented impact on gefitinib pharmacokinetics. CYP3A4 emerged as the dominant modifier: approximately half of the cohort carried a CYP3A4 variant associated with reduced gefitinib metabolism. CYP3A4 is the principal enzyme responsible for gefitinib clearance, and this analysis defined metaboliser status as the axis along which to select cell lines.

2.2 Phenotypic characterisation and selection of hepatocyte lines

Six iPSC-derived hepatocyte (iHep) lines were screened by Cytochroma using cell painting, a high-content imaging assay in which a cocktail of fluorescent dyes labels the nucleus, endoplasmic reticulum, Golgi apparatus, cytoskeleton, mitochondria and RNA simultaneously, so that automated microscopy yields a multidimensional morphological signature for every cell in the sample [8]. Representative images at low and high gefitinib doses are shown in Figure 3.

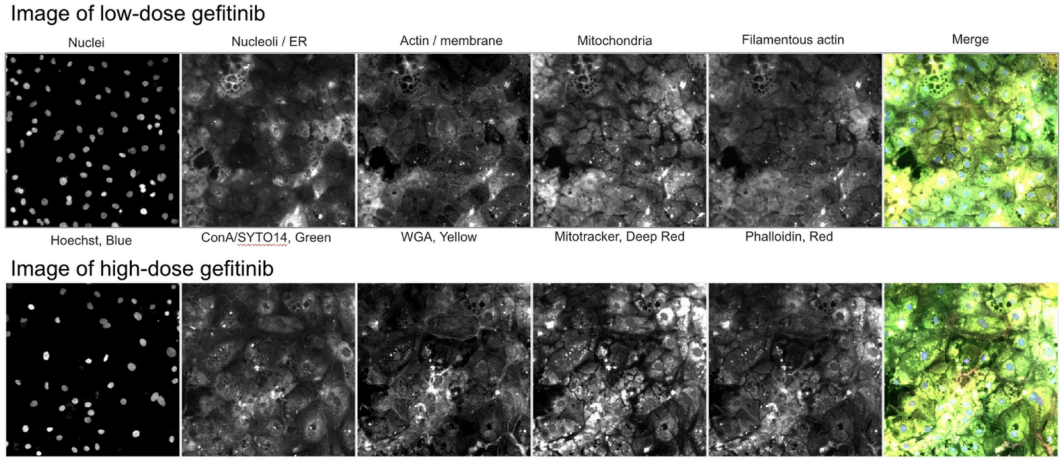

Figure 3: Representative cell painting data generated by Cytochroma for gefitinib-treated iHeps at low dose (top) and high dose (bottom). Channels, left to right: nuclei (Hoechst), nucleoli/ER (ConA/SYTO14), actin and membrane (WGA), mitochondria (MitoTracker), filamentous actin (phalloidin), and merged composite.

CYP3A4 activity was quantified for each line by luminogenic assay and reported as relative light units (RLU; Figure 4). Donor sex and genetic ancestry proportions were also considered, with the explicit aim of selecting female donors, which remain under-represented in in vitro toxicology, and of covering ancestries whose allele frequencies differ from those of the predominantly Western lines used in most published work (Table 1).

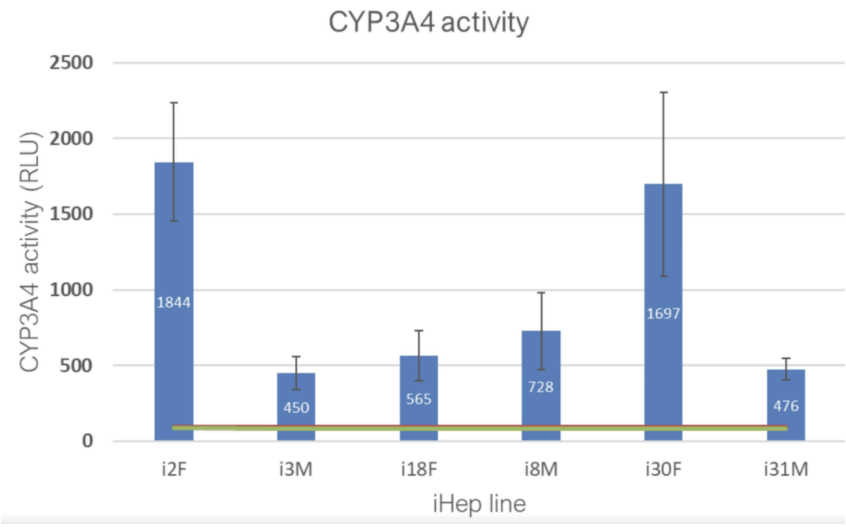

Figure 4: CYP3A4 activity (Relative Light Units) across the six screened iHep lines. i18F (565 RLU) and i30F (1,697 RLU) were selected as the low- and high-activity pair.

Table 1: Donor panel: sex, genetic ancestry proportions and CYP3A4 activity. Selected lines in bold.

iHep line	Sex	African	European	Native American	CYP3A4 (RLU)
i2F	F	0.240	0.720	0.020	1,844
i3M	M	0.190	0.780	0.030	450
i8M	M	0.551	0.378	0.071	728
i18F	F	0.192	0.244	0.565	**565**
i30F	F	0.269	0.454	0.277	**1,697**
i31M	M	0.016	0.727	0.257	476

This analysis resulted in the selection of **i18F**, a female line with low CYP3A4 activity and a predominantly Native American ancestry component, and **i30F**, a female line with approximately three-fold higher CYP3A4 activity and the larger European ancestry component of the two (0.454 versus 0.244). The pair therefore varies along the axis of interest, metabolic capacity, while also sampling two ancestry backgrounds with different population prevalence.

2.3 Gefitinib treatment and transcriptomic profiling

Both lines were treated with gefitinib at 0.3, 1, 3, 10 and 30 µM, alongside a DMSO vehicle control. mRNA was extracted and sequenced; data were quality controlled and pre-processed, and differential expression was computed against the matched vehicle control at each concentration. Log2 fold changes and Benjamini-Hochberg adjusted p-values were used as input to gene set enrichment analysis (GSEA) [9] against the WikiPathways 2021 Human collection [10], and to the network inference steps described below. The clinically relevant plasma maximum concentration of gefitinib at 250 mg/day is approximately 0.3-1 µM, so the lower concentrations sit within the therapeutic window and 30 µM represents a deliberately supra-therapeutic challenge.

2.4 Pathway, transcription factor and causal network inference

Transcription factor activities were estimated from the differential expression signatures using a regulon-based footprint approach [11, 12], and pathway activities using perturbation-response signatures [13]. Causal networks linking assumed upstream targets to inferred transcription factor activity were reconstructed with CARNIVAL [14] under three prior configurations: PRKD1 alone, PRKD1 together with EGFR, and an inverse formulation with no upstream target prior. Comparing these runs allows the contribution of the target assumption to be separated from the contribution of the data, and provides a check on how strongly the inferred topology depends on prior belief.

2.5 Target prediction for gefitinib metabolites

Gefitinib metabolites reported by Liu et al. [15] were submitted to CELLSCAPE, our structure-based target prediction tool, to obtain predicted probabilities of engagement across a panel of approximately 2,000 human proteins at 10 and 100 µM. This step was included to test whether metabolites , rather than the parent compound,could plausibly account for the response observed in the high-metabolising line.

3 Results

3.1 Global transcriptional trajectories diverge with metabolic capacity

Principal component analysis of the full expression matrix separates the two lines along divergent trajectories (Figure 5). PC1 accounts for 58.5% of variance and is dominated by concentration, PC2 accounts for a further 20.1% and separates the two cell lines at high dose. Up to 3 µM the samples cluster tightly near the origin, but from 10 µM onwards the two lines move in opposite directions along PC2, ending at (50, +21) for i18F and (36, -28) for i30F at 30 µM. The magnitude of displacement is comparable, but the direction is not: the two lines are not simply at different points on a shared dose-response, they are mounting qualitatively different responses.

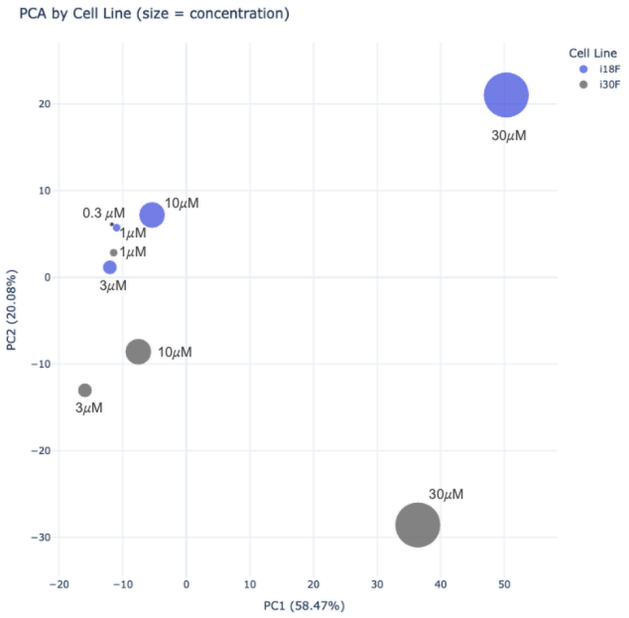

Figure 5: PCA of gene expression for i18F and i30F treated with gefitinib at 0.3-30 µM; marker size encodes concentration. The two lines follow divergent trajectories at 10 and 30 µM.

3.2 i18F: signalling collapse and loss of metabolic competence

In the low-metabolising line, increasing gefitinib concentration produces a progressive, largely down-regulatory response (Figure 6). CYP1A1 rises monotonically and is the dominant up-regulated transcript at 30 µM, indicating that the cell senses the chemical load and attempts to compensate by inducing cytochrome P450 production; sustained high CYP1A1 expression has itself been linked to hepatotoxicity through reactive oxygen species generation. AGR2, a marker of tumour progression associated with EGFR signalling, is strongly down-regulated, consistent with effective target engagement, and LIN28A declines with dose, indicating loss of proliferative capacity. UGT2B11 also falls, consistent with reports that EGFR inhibition reduces expression of UGT genes.

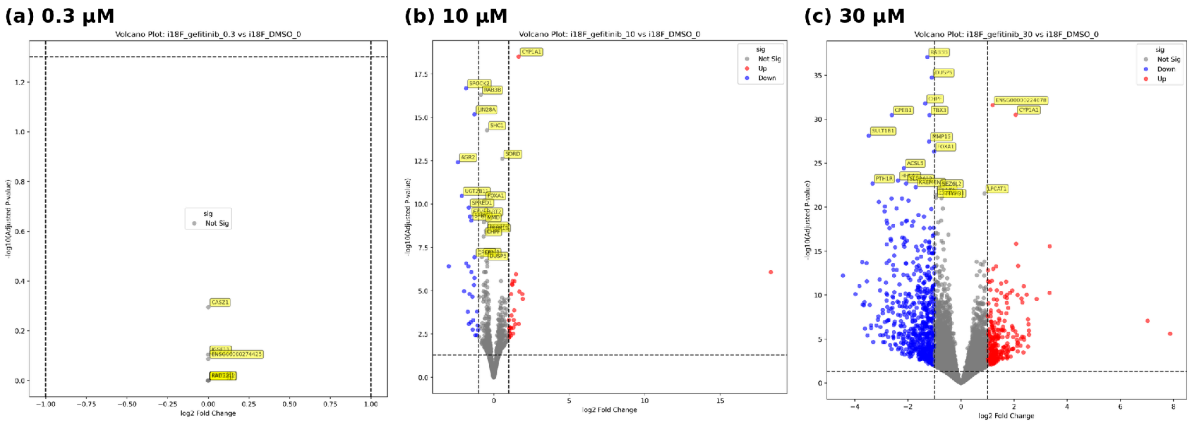

Figure 6: Differential expression in i18F (low CYP3A4) versus DMSO control at (a) 0.3 µM, (b) 10 µM and (c) 30 µM gefitinib. Blue, significantly down-regulated; red, significantly up-regulated; grey, not significant.

At 30 µM the pattern is best described as signalling collapse. The two most significant down-regulated genes are **RAB3B**, a vesicle transport and cell-surface protein regulator whose loss indicates a breakdown of structural and secretory integrity, and **DUSP5**, a negative regulator of the MAPK/ERK pathway whose down-regulation indicates that the EGFR-driven survival pathway has been comprehensively neutralised. Phase II conjugation is also lost: **SULT1B1**, which catalyses the sulfation reactions that render drugs water-soluble for excretion, is among the most strongly suppressed transcripts, so the cell has lost that detoxification route at precisely the point it is most needed. **LPCAT1**, a reported marker of gefitinib resistance in lung adenocarcinoma that acts through an LPCAT1-EGFR positive feedback loop [16], appears on the up-regulated side, suggesting that a subset of cells attempts to activate lipid-mediated survival signalling to bypass the blocked EGFR pathway.

3.3 i30F: a high-output metabolic response with genotoxic features

The high-metabolising line shows a larger number of differentially expressed genes overall and a more structured response (Figure 7). At 1 µM the field of significant genes is already noticeably more crowded than in i18F at the same dose: SPOCK2, LIN28A and ONECUT2 are significantly down-regulated, so gefitinib is reaching its target despite high CYP activity, while CYP1A1 is not yet a top hit - at this concentration the line is clearing the drug using existing enzyme levels rather than inducing new production.

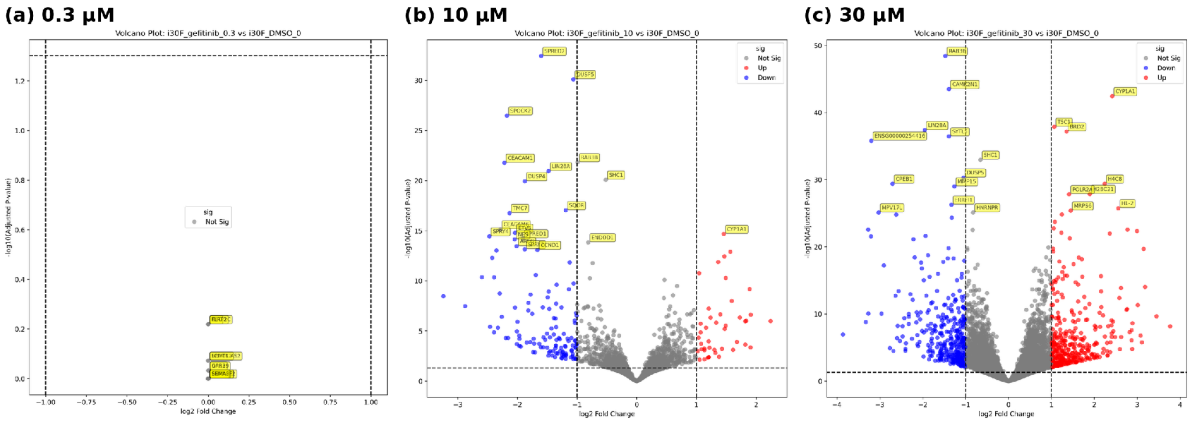

Figure 7: Differential expression in i30F (high CYP3A4) versus DMSO control at (a) 0.3 µM, (b) 10 µM and (c) 30 µM gefitinib. Note the larger number of significant genes and the broad cluster of up-regulated transcripts accompanying CYP1A1 at the higher concentrations.

By 10 µM the line enters a state of simultaneous signalling inhibition and metabolic induction. CYP1A1 is accompanied by a broad cluster of up-regulated genes rather than standing alone as it does in i18F, indicating a genuine increase in metabolic output. SPRED2 and DUSP5, both negative regulators of MAPK, are highly significant, reflecting an active attempt to modulate the signalling flux that gefitinib is blocking, and the high significance of SHC1, a key adaptor for EGFR, suggests the line is rewiring its growth factor signalling scaffold.

At 30 µM CYP1A1 reaches its highest level and two features distinguish the response from that of i18F. First, **ERRFI1**, a potent negative feedback regulator of EGFR, is significantly down-regulated, indicating active remodelling of EGFR feedback control - a release of negative feedback on the pathway the drug is blocking - rather than the indiscriminate loss of regulators seen in i18F. Second, several histone genes - **H4C8**, **H2BC21** and **H1-2** - are among the most strongly up-regulated transcripts. Changes in histone expression typically accompany chromatin remodelling in response to DNA damage, and their appearance here is the first indication of genotoxic stress specific to the high-metabolising line.

3.4 Pathway enrichment: a shared sphingolipid core and a divergent stress response

GSEA at 30 µM makes the divergence explicit (Figure 8). In i18F, every significantly enriched WikiPathways term is negatively enriched. The most strongly suppressed sets are Glycolysis and Gluconeogenesis, Constitutive Androstane Receptor, Metapathway Biotransformation Phase I and II (NES approximately -1.9), Pregnane X Receptor, Nuclear Receptors in Lipid Metabolism and Toxicity, PPAR signalling, Farnesoid X Receptor, the Nuclear Receptors Meta-Pathway, the NRF2 pathway and Globo Sphingolipid Metabolism (NES approximately -1.75). This is the transcriptional signature of a hepatocyte losing function on every axis simultaneously: it can neither biotransform the drug, nor maintain lipid and bile acid regulation, nor sustain energy metabolism. Suppression of complex sphingolipid synthesis is of particular interest, since in many models this leads to accumulation of pro-apoptotic ceramides.

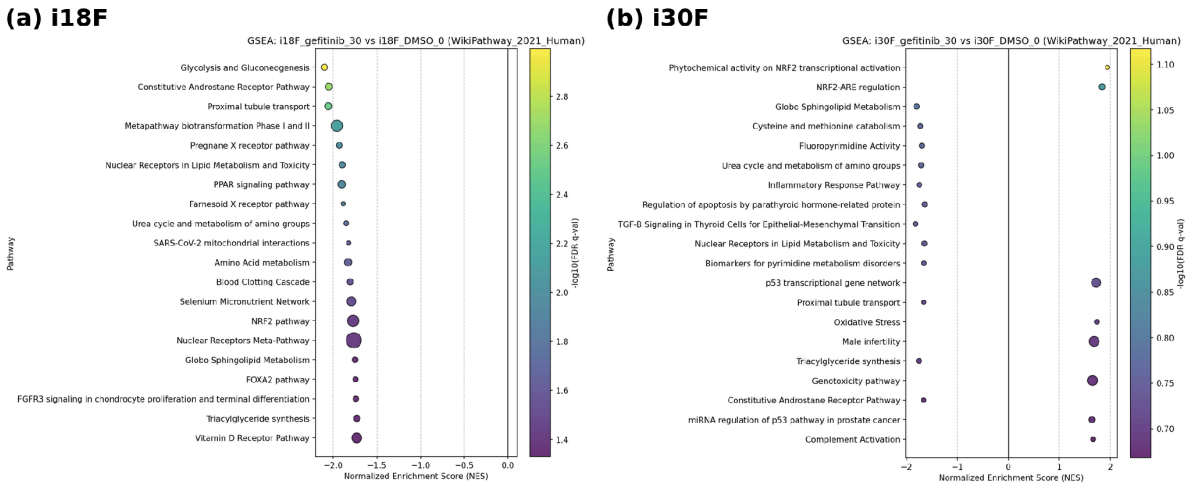

Figure 8: GSEA (WikiPathways 2021 Human) at 30 µM gefitinib versus DMSO for (a) i18F and (b) i30F. Marker size encodes -log10 FDR q-value. All enriched terms in i18F are negative; i30F combines negative sphingolipid and nuclear receptor enrichment with positive NRF2, oxidative stress, p53 and genotoxicity enrichment.

In i30F the picture is bidirectional. Globo Sphingolipid Metabolism is again negatively enriched (NES approximately -1.8), together with Nuclear Receptors in Lipid Metabolism and Toxicity, triacylglyceride synthesis, urea cycle and inflammatory response terms. On the positive side, however, sit NRF2-ARE regulation, phytochemical activity on NRF2 transcriptional activation, the p53 transcriptional gene network, Oxidative Stress and, notably, the Genotoxicity pathway - a term entirely absent from the i18F results. Selected terms are summarised in Table 2.

Table 2: Selected WikiPathways terms at 30 µM gefitinib. Arrows indicate the direction of normalised enrichment; "-" indicates the term was not among the significantly enriched sets for that line.

Pathway	i18F	i30F	Interpretation
Globo sphingolipid metabolism	down	down	Shared core response; consistent with PRKD1 inhibition
Metapathway biotransformation Phase I/II	down	-	Loss of biotransformation capacity in i18F
Nuclear receptors in lipid metabolism and toxicity	down	down	Disruption of lipid regulatory machinery
Glycolysis and gluconeogenesis	down	-	Energy metabolism failure in i18F
PPAR / FXR / PXR / CAR	down	partial	Cholestasis and steatosis liability
NRF2 pathway / NRF2-ARE regulation	down	up	Electrophilic stress response only in i30F
Oxidative stress	-	up	Reactive metabolite burden
p53 transcriptional gene network	-	up	DNA damage response
Genotoxicity pathway	-	up	Absent in i18F; metabolite-associated

The shared negative enrichment of globo sphingolipid metabolism in both lines of human iPSC-derived hepatocytes is an independent transcriptional confirmation of the mechanism our earlier case study identified in primary rat hepatocytes and validated by kinase assay [5]. The two lines seem to handle the consequences differently: i18F loses lipid homeostasis alongside a collapse of biotransformation, whereas i30F suppresses the same lipid pathways while actively mounting NRF2- and p53-dependent defences.

3.5 NRF2 target gene induction supports a reactive-metabolite burden in i30F

NRF2 (NFE2L2) is the master cellular sensor for electrophiles and oxidative damage. Under basal conditions KEAP1 targets NRF2 for ubiquitin-mediated degradation; electrophilic modification of KEAP1 cysteines releases NRF2, which translocates to the nucleus, dimerises with small Maf proteins and transactivates antioxidant response element (ARE)-containing genes. We therefore examined the NRF2 regulon directly rather than relying on the pathway-level score (Figure 9).

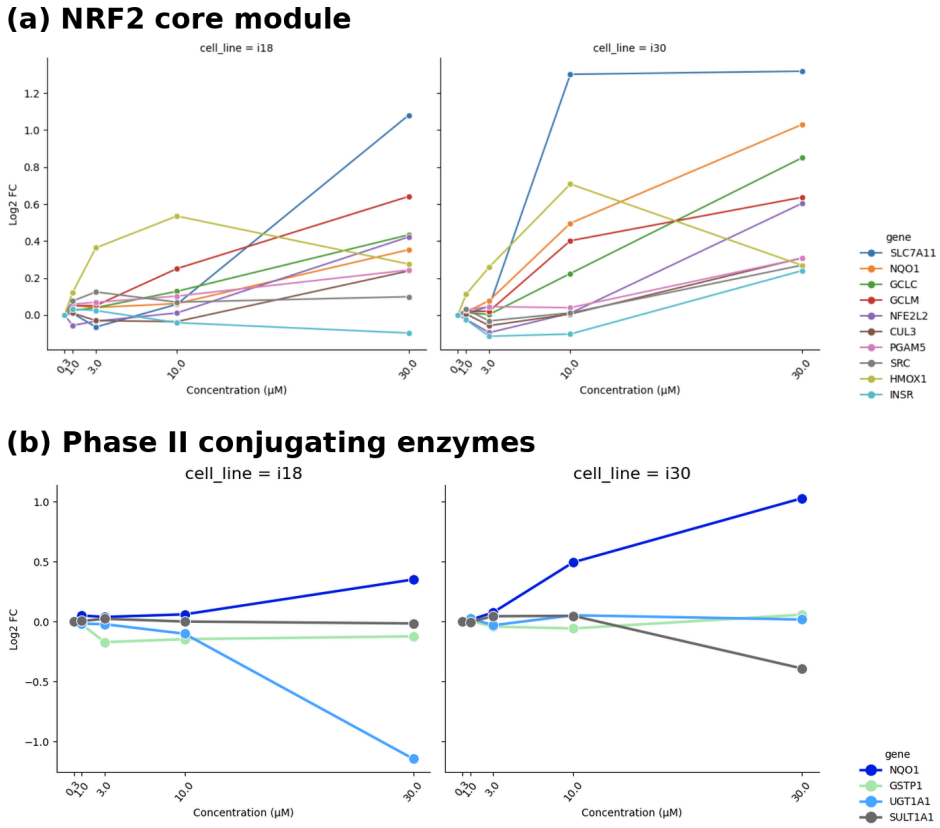

Figure 9: Log2 fold change versus DMSO control across gefitinib concentrations for (a) the NRF2 core module and (b) Phase II conjugating enzymes, in i18 (left) and i30 (right) panels.

The NRF2 core module is induced in both lines but consistently more strongly in i30F. At 30 µM, SLC7A11 reaches +1.32 in i30F against +1.08 in i18F, NQO1 +1.03 against +0.35, GCLC +0.85 against +0.43, and NFE2L2 itself +0.60 against +0.42. The kinetics also differ: in i30F, SLC7A11 is already saturated at 10 µM (+1.30) and HMOX1 peaks at 10 µM (+0.71) before partially resolving, the profile expected of an adaptive response engaged early and then maintained. NQO1 is of specific mechanistic interest because its primary function is the two-electron reduction of quinones to less toxic hydroquinones; its strong induction in the high-metabolising line is consistent with the cell sensing a quinone-imine burden and increasing capacity to neutralise it. SRXN1 and HMOX1, both canonical downstream NRF2 reporters, behave as described for

electrophilic compounds in liver cells by ter Braak et al. [17], supporting an interpretation of electrophilic protein stress rather than direct DNA damage as the initiating event.

Phase II conjugation separates the two lines even more clearly. In i18F, UGT1A1 falls to -1.15 at 30 µM while GSTP1 and SULT1A1 remain flat, so the only Phase II enzyme induced is NQO1 and the dominant conjugation route is lost. In i30F, UGT1A1 and GSTP1 are stable to marginally increased and NQO1 is strongly induced; only SULT1A1 declines (-0.40). The glutathione synthesis, efflux, antioxidant and repair modules downstream of NRF2 follow the same asymmetry.

3.6 Transcription factor activity is dominated by cell line, not by dose

Inference of transcription factor (TF) activity across all conditions shows that the dominant source of variation is the cell line rather than the concentration or the choice of network prior (Figure 10). In i18F, AP-1 components (JUN, FOS and their dimers) are positively active at 0.3 µM - the earliest sign of a stress response in either line - and ZMYND8, a chromatin regulator involved in the DNA damage response, is strongly active at 1 µM. At 30 µM, HNF1A becomes strongly negative, indicating loss of hepatocyte identity. In i30F the pattern is one of broad, deep inhibition at intermediate concentrations: ETS1, CTNNB1, SMAD3, SMAD4, BCL3 and BACH1 all reach strongly negative activity at 3-10 µM (ETS1 approximately -11 at 10 µM), implicating TGF-β and Wnt signalling in the response of the high-metabolising line.

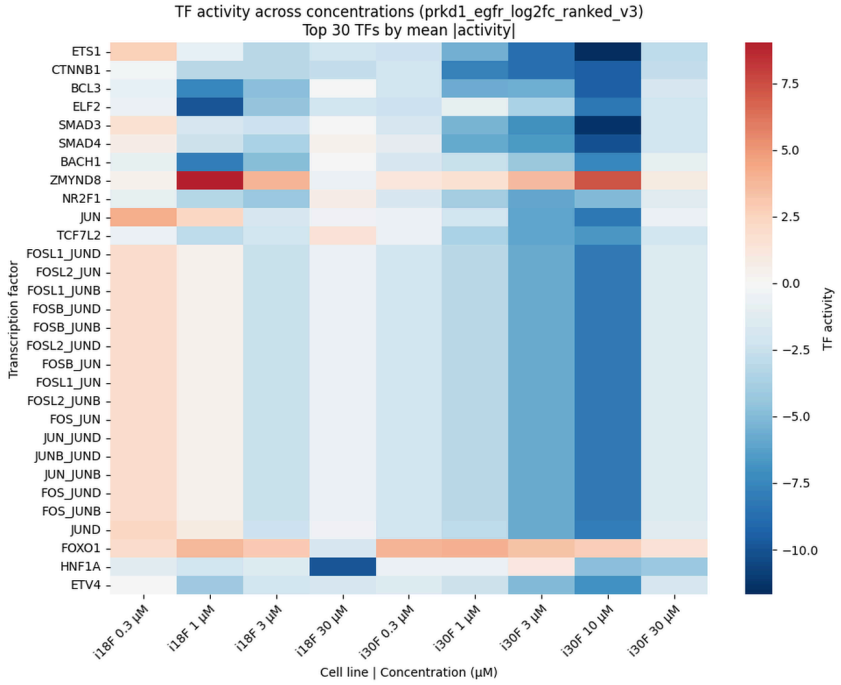

Figure 10: Inferred transcription factor activity (top 30 TFs by mean absolute activity) across cell lines and concentrations. Red, increased activity; blue, decreased activity.

Footprint-based pathway activities are consistent with gefitinib acting as an EGFR inhibitor, with EGFR and MAPK activity negative in both lines and more strongly negative in i30F (Table 3). The concentration profiles differ between the lines in the same direction as the differentially expressed genes: p53 activity in i18F is elevated from 0.3 µM and declines by 30 µM, whereas in i30F it is low at low concentrations and reaches its maximum (+6.5) at 30 µM. Two conditions - i18F at 0.3 µM for EGFR and at 30 µM for MAPK - return positive scores that run against the overall trend; we do not interpret these individually. Overall the pattern is of

early stress signalling in i18F and late, sharp stress in i30F, which is what would be expected if lower CYP3A4 activity increases effective exposure to the parent compound at any given nominal dose.

Table 3: Footprint-inferred pathway activity by cell line and concentration. Negative values indicate inferred inhibition. "-" indicates no solution for that condition.

Pathway / line	0.3 µM	1 µM	3 µM	10 µM	30 µM
EGFR, i18F	+6.23	-0.26	-2.46	-	-3.70
EGFR, i30F	-1.99	-5.00	-7.08	-12.24	-4.44
MAPK, i18F	-3.09	-5.60	-8.31	-	+2.33
MAPK, i30F	-4.29	-14.62	-8.76	-9.01	-1.39
p53, i18F	+3.02	+3.85	+3.91	-	+2.02
p53, i30F	+2.42	+1.76	0.00	+4.07	+6.54

3.7 Causal network inference requires an EGFR prior

Causal network reconstruction was attempted with CARNIVAL under three priors: PRKD1 alone, PRKD1 together with EGFR, and a formulation with no upstream target prior. Only the PRKD1+EGFR prior returned solutions at every concentration; PRKD1 alone and the prior-free formulation failed to converge for many conditions, and where they did converge they implicated different upstream drivers. Ranked pathway involvement was nonetheless stable across all three runs (MAPK > EGFR > JAK-STAT > TGF-β > p53 > PI3K). We draw one conclusion from this and no more: EGFR must be included as an upstream target for the data to be explained, which supports it as the dominant driver of the transcriptional response, while PRKD1 alone is insufficient - a statement about the transcriptional footprint rather than about target engagement. Because pathway and transcription factor activities are identical across the three runs and only the inferred topology changes, individual edges and network sizes are too prior-dependent to interpret, and we do not do so here.

3.8 Metabolite target prediction offers a candidate source of genotoxic stress

If the distinguishing feature of i30F is a burden of reactive metabolites, those metabolites should be identifiable and should have plausible targets. Liu et al. [15] characterised gefitinib biotransformation by CYP3A4 and CYP1A2, describing the formation of M1, M2 and M26 alongside two aldehyde-bearing species, M18 and M20, formed by oxidative opening of the propoxy-morpholine side chain (Figure 11). Both are hard electrophiles capable of reacting with DNA or with protein amino acid side chains, and are therefore candidates for the electrophilic stress inferred from the NRF2 response.

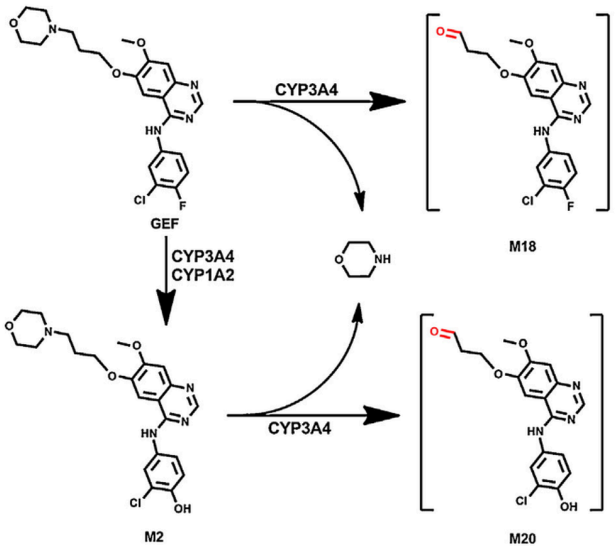

Figure 11: CYP3A4- and CYP1A2-mediated formation of the aldehyde metabolites M18 and M20 from gefitinib (GEF) and its O-demethylated metabolite M2, with release of morpholine. Adapted from Liu et al. [15].

CELLSCAPE predictions for these four metabolites (Figure 12) indicate that M1 and M2 behave as polytarget inhibitors, engaging EGFR, EPHB4, RET, BRAF, MKNK1, RIPK2, KDR, ERBB3, ABL1 and AURKB above the 0.7 probability threshold. Inhibition of AURKB or ABL1 at clinically achievable concentrations could interfere with DNA repair and mitosis, providing a route to secondary genotoxic effects. M18 and M20 have narrower predicted profiles centred on EGFR, ERBB2, EPHB4 and KDR. KDR (VEGFR2) inhibition is of interest here because it is frequently associated with mitochondrial dysfunction and a consequent rise in reactive oxygen species - a mechanism that would be expected to activate NRF2. These predictions are structure-based and require experimental confirmation, but they provide a concrete, testable link between elevated CYP3A4 activity and the oxidative and genotoxic signature observed in i30F.

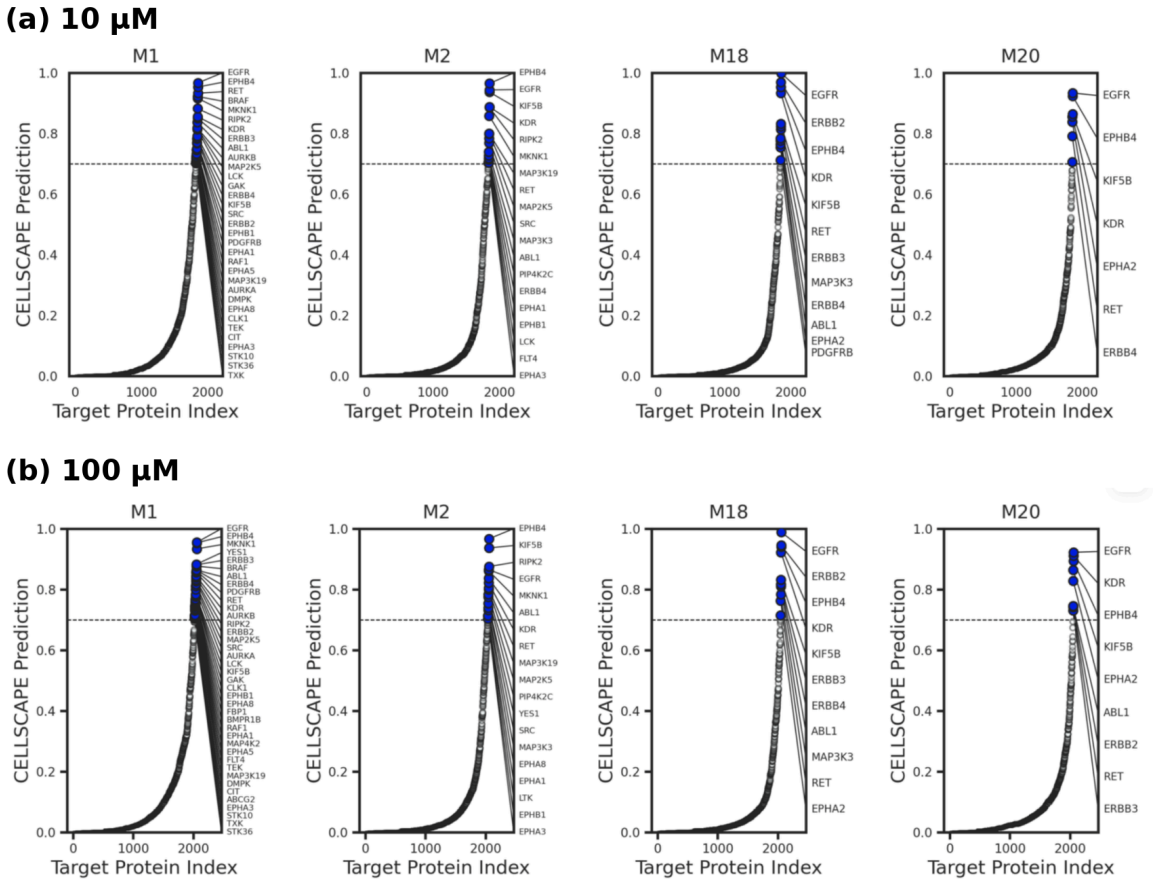

Figure 12: CELLSCAPE predicted target engagement for gefitinib metabolites M1, M2, M18 and M20 at (a) 10 µM and (b) 100 µM. Blue points exceed the 0.7 probability threshold; the dashed line marks that threshold.

3.9 Alignment with population-level genomics

The NRF2-mediated signature is specific to i30F, the line with the larger European ancestry component (0.454 versus 0.244). This cellular divergence mirrors a documented genomic divide in NSCLC. KEAP1 loss-of-function mutations, the principal trigger for constitutive NRF2 activation, occur in approximately 12-15% of European patients but in only 0.5-0.9% of East Asian patients [18], whereas East Asian cohorts are instead dominated by EGFR mutations and by T790M- or BIM-mediated resistance (Table 4) [19]. Disruption of the KEAP1-NRF2 axis has been shown directly to confer gefitinib resistance and cross-resistance to the irreversible EGFR-TKIs afatinib and osimertinib in human lung cancer cells [20].

Table 4: Reported mutation frequencies in NSCLC by population. Values from Izumi et al. [19]; note that the KEAP1 adenocarcinoma frequency reported there (17.8% Caucasian) is higher than the 12-15% range cited for European cohorts by Zavitsanou et al. [18].

Feature	East Asian	Caucasian
EGFR mutation frequency	~51.1%	~14.6%
KEAP1 mutations (adenocarcinoma)	~0.5%	~17.8%
KEAP1 mutations (squamous cell)	~0.9%	~12.7%
NFE2L2 (NRF2) mutations	~13.6%	~15.8%

By isolating an NRF2-dependent toxicity and survival mechanism in a line with greater European genetic proximity, and its absence in a line with predominantly Native American ancestry, this work identifies a candidate population-specific toxicity profile. It offers a mechanistic rationale for why NRF2-linked gefitinib resistance is disproportionately reported in Western clinical settings, and it illustrates the practical consequence of the field's reliance on a narrow set of donor backgrounds. We emphasise that ancestry proportions in two iPSC lines are not a substitute for a genetically stratified cohort; the alignment is suggestive and motivates a targeted clinical analysis rather than settling one.

4 Interpretation: two routes to the same clinical endpoint

The results support a model in which CYP3A4 activity does not simply scale the severity of gefitinib hepatotoxicity but changes its character, because it changes the ratio of parent compound to reactive metabolite at any given exposure.

Published mechanistic work on gefitinib hepatotoxicity has variously implicated CYP450-dependent bioactivation [22], mitochondrial and endoplasmic reticulum stress with caspase activation [23], and PLK1-dependent autophagy [24]. Our results do not contradict any of these; they suggest that which mechanism dominates may depend on the metaboliser context in which the drug is handled.

In **i18F**, low CYP3A4 activity means the parent compound persists. Effective intracellular exposure is therefore higher than the nominal dose implies, which explains why stress-associated transcription factors and pathways - AP-1, p53, NF-κB components and ATF4 - are already elevated at 0.3-1 μM in this line and not in i30F. As concentration increases, the cell attempts compensation through CYP1A1 induction and, late and unsuccessfully, through LPCAT1-mediated membrane remodelling, but Phase I and II biotransformation collapse, hepatocyte identity factors (HNF1A, HNF4A) are suppressed, and metabolic nuclear receptor signalling (PPAR, RXR, FXR) is lost - a combination that carries cholestasis and steatosis liability and that has been described in other DILI settings [21]. Suppression of glycolysis and gluconeogenesis alongside these changes is what would be expected of a hepatocyte losing viability; inhibition of anaerobic glycolysis has been reported as a mechanism of injury for other hepatotoxic drugs [25].

In **i30F**, high CYP3A4 activity clears the parent compound efficiently but generates aldehyde and quinone-imine species in the process. The transcriptional consequence is not passive failure but active defence: NRF2-ARE induction, glutathione synthesis, NQO1 and efflux pump up-regulation, and p53 activation. The cost of this strategy appears at 30 μM as positive enrichment of the genotoxicity pathway and up-regulation of histone genes - the signature of a line that copes well until the metabolic route itself becomes the source of injury. This dichotomy is consistent with the clinical observation that gefitinib hepatotoxicity varies with metaboliser phenotype and that patients intolerant of gefitinib can sometimes be switched successfully to erlotinib [3].

Superimposed on both is the off-target mechanism identified in our earlier work. PRKD1 is a master regulator of Golgi-to-plasma-membrane transport, and its inhibition would be expected to disrupt secretory trafficking. The severe down-regulation of **RAB3B** in both lines - the single most significant down-regulated gene at 30 μM in each - together with the loss of secreted and surface-associated transcripts such as AGR2, is consistent with such a footprint, as is the shared suppression of globo sphingolipid metabolism. We regard this as supporting evidence rather than proof: RAB3B loss is compatible with PRKD1 inhibition but is not specific to it. Table 5 summarises the comparison.

Table 5: Comparative summary of the two phenotypes at 30 µM gefitinib.

Feature	i18F (low CYP3A4)	i30F (high CYP3A4)
Dominant species	Parent compound	Reactive metabolites
Earliest stress signal	AP-1, p53 at 0.3-1 µM	10-30 µM
CYP1A1	Induced, isolated peak	Maximised within a broad up-regulated cluster
Phase II capacity	Lost (SULT1B1, UGT1A1, UGT2B11 down)	Retained; NQO1 strongly induced
NRF2 axis	Negatively enriched	Positively enriched; SLC7A11, NQO1, GCLC induced
p53 / genotoxicity	p53 early, falls by 30 µM; no genotoxicity term	p53 peaks at 30 µM; genotoxicity enriched
Hepatocyte identity TFs	HNF1A strongly suppressed	Moderate suppression
Sphingolipid metabolism	Down	Down
RAB3B	Severe down-regulation	Down-regulation
Overall phenotype	Passive metabolic collapse	Active defence with genotoxic cost

5 Clinical Relevance

If the two mechanisms described here operate in patients, they have different clinical implications and are not managed in the same way. For slow metabolisers, the risk is cumulative parent-compound exposure with progressive loss of hepatic metabolic competence; the relevant interventions are dose adjustment guided by CYP3A4 genotype or phenotype, avoidance of concomitant CYP3A4 inhibitors, and monitoring of liver function with attention to cholestatic as well as hepatocellular patterns. For fast metabolisers, the risk is not insufficient clearance but the electrophilic and genotoxic burden that efficient clearance generates; here dose reduction alone may be a less reliable safeguard, and markers of oxidative stress or glutathione depletion may be more informative than transaminases alone.

The population dimension is directly actionable in trial design. If NRF2-dependent mechanisms are enriched in patients of European ancestry and largely absent in others, then safety and resistance signals observed in one population should not be assumed to transfer, and stratification by KEAP1-NRF2 status is worth considering prospectively. More broadly, the fact that a mechanism of this significance emerged only once female and non-European donor lines were included is an argument for building donor diversity into preclinical safety panels as a matter of routine rather than as a follow-up study.

6 Limitations

- **Two donor lines.** Ancestry proportions in two iPSC lines cannot support population-level inference. The alignment with KEAP1-NRF2 epidemiology is a hypothesis, not a demonstration, and cell-intrinsic differences unrelated to CYP3A4 or ancestry cannot be excluded.
- **Transcriptomic readouts only.** Pathway and network activities are inferred from gene expression. No viability, ATP, glutathione, ROS, adduct or DNA damage endpoint was measured, so stress signatures and network contraction are indirect evidence of toxicity.
- **Unmatched conditions.** Not every concentration yielded a solution in every network run, which limits direct like-for-like comparison between lines at some doses.

- **Prior sensitivity.** Inferred network topology depends materially on the assumed upstream target. Networks obtained under the PRKD1+EGFR prior should not be read as target-agnostic evidence for either target.
- **Predicted, not measured, metabolite targets.** CELLSCAPE predictions for M1, M2, M18 and M20 are structure-based. The metabolites were not quantified in these cells, and their predicted targets were not assayed here.
- **iPSC-derived hepatocytes.** These lines are not primary human hepatocytes and may differ in absolute CYP expression, so pathway activities may not translate directly to the human liver in vivo.

7 Implications for Future Research

The findings define a compact validation programme. Direct measurement of M18 and M20 in both lines, paired with glutathione and protein adduct quantification, would establish whether the NRF2 signature in i30F is genuinely metabolite-driven. Comet or γH2AX assays at 0.3-1 μM in the high-metabolising line would test whether the genotoxic signature extends into the therapeutic window, which is the finding with the greatest clinical consequence if confirmed. Kinase assays against AURKB, ABL1 and KDR for the isolated metabolites would test the CELLSCAPE predictions. CYP3A4 knockdown in i30F and induction in i18F would establish whether metaboliser status alone is sufficient to switch the phenotype between the two patterns described here, separating it from other donor differences. Direct lipidomic measurement of ceramide and sphingosine-1-phosphate would convert the shared sphingolipid enrichment from a transcriptional inference into a measured metabolic change.

More broadly, this study illustrates a workflow - pharmacogenomic cohort analysis to select the axis of variation, phenotypic screening to select the models, concentration-resolved transcriptomics to characterise the response, and causal inference plus structure-based prediction to generate mechanism - that is applicable to any compound whose toxicity is heterogeneous across patients. Extending it across the EGFR-TKI class would test whether the parent-compound and reactive-metabolite routes described here are specific to gefitinib or general to the class.

8 Conclusion

Two donor-diverse, female iPSC-derived hepatocyte lines with a three-fold difference in CYP3A4 activity respond to gefitinib in qualitatively different ways. Both suppress globo sphingolipid metabolism, independently reproducing in human cells the PRKD1-linked mechanism our earlier case study predicted and validated. Beyond that shared core, the low-metabolising line accumulates parent compound and undergoes a passive collapse of biotransformation, hepatocyte identity and energy metabolism, while the high-metabolising line mounts an NRF2- and p53-dependent defence and pays for it in oxidative and genotoxic stress at high concentration. Structure-based prediction identifies the aldehyde metabolites M18 and M20, and the polytarget metabolites M1 and M2, as plausible sources of that stress. That the NRF2 mechanism appears in the line with greater European ancestry, and that KEAP1-NRF2 alterations are an order of magnitude more frequent in Western than in East Asian NSCLC cohorts, points to a population-specific toxicity profile with consequences for how EGFR-TKI safety is studied and stratified. These results are early and require the experimental validation set out above, but they indicate that a single drug can injure the liver by more than one route, and that which route a given patient takes may be written in their pharmacogenome.

References

[1] M. Chen, A. Suzuki, S. Thakkar, K. Yu, C. Hu, and W. Tong, "DILIrank: the largest reference drug list ranked by the risk for developing drug-induced liver injury in humans," *Drug Discov Today*, vol. 21, pp. 648-653, Apr 2016.

[2] National Institute of Diabetes and Digestive and Kidney Diseases, *Gefitinib. LiverTox: Clinical and Research Information on Drug-Induced Liver Injury*. Bethesda (MD): National Library of Medicine (US), 2018.

[3] T. Kijima, H. Shimizu, et al., "Safe and successful treatment with erlotinib after gefitinib-induced hepatotoxicity," *J Clin Oncol*, vol. 29, 2011. doi:10.1200/JCO.2010.34.3368.

[4] U.S. Food and Drug Administration, *FDA Adverse Event Reporting System (FAERS) Public Dashboard*. Accessed 2026.

[5] L. Hosseini-Gerami, S. Masarone, and J. Lane, "Using SAFEPATH to uncover a novel mechanism of hepatotoxicity for gefitinib," *bioRxiv*, 2024. doi:10.1101/2024.07.31.605988.

[6] L. Li, H. Wang, and J. W. Jones, "Sphingolipid metabolism as a marker of hepatotoxicity in drug-induced liver injury," *Prostaglandins Other Lipid Mediat*, vol. 151, p. 106484, Dec 2020.

[7] M. Whirl-Carrillo, E. M. McDonagh, J. M. Hebert, et al., "Pharmacogenomics knowledge for personalized medicine," *Clin Pharmacol Ther*, vol. 92, pp. 414-417, 2012.

[8] M.-A. Bray, S. Singh, H. Han, et al., "Cell Painting, a high-content image-based assay for morphological profiling using multiplexed fluorescent dyes," *Nat Protoc*, vol. 11, pp. 1757-1774, 2016.

[9] A. Subramanian, P. Tamayo, V. K. Mootha, et al., "Gene set enrichment analysis: a knowledge-based approach for interpreting genome-wide expression profiles," *PNAS*, vol. 102, no. 43, pp. 15545-15550, 2005.

[10] M. Martens, A. Ammar, A. Riutta, et al., "WikiPathways: connecting communities," *Nucleic Acids Res*, vol. 49, pp. D613-D621, 2021.

[11] L. Garcia-Alonso, C. H. Holland, M. M. Ibrahim, D. Turei, and J. Saez-Rodriguez, "Benchmark and integration of resources for the estimation of human transcription factor activities," *Genome Res*, vol. 29, pp. 1363-1375, 2019.

[12] P. Badia-i-Mompel, J. Velez Santiago, J. Braunger, et al., "decoupleR: ensemble of computational methods to infer biological activities from omics data," *Bioinformatics Advances*, vol. 2, 2022.

[13] M. Schubert, B. Klinger, M. Klunemann, et al., "Perturbation-response genes reveal signaling footprints in cancer gene expression," *Nat Commun*, vol. 9, p. 20, 2018.

[14] A. Liu, P. Trairatphisan, E. Gjerga, et al., "From expression footprints to causal pathways: contextualizing large signaling networks with CARNIVAL," *NPJ Syst Biol Appl*, vol. 5, p. 40, 2019.

[15] X. Liu, Y. Lu, X. Guan, et al., "Metabolomics reveals the formation of aldehydes and iminium in gefitinib metabolism," *Biochem Pharmacol*, vol. 97, pp. 111-121, 2015.

[16] J. Ding, X. Ding, and Z. Leng, "LPCAT1 promotes gefitinib resistance via upregulation of the EGFR/PI3K/AKT signaling pathway in lung adenocarcinoma," *J Cancer*, vol. 13, pp. 1837-1848, 2022.

[17] B. ter Braak, S. Wink, E. Koedoot, et al., "Mapping the dynamics of Nrf2 antioxidant and NF-κB inflammatory responses by soft electrophilic chemicals in human liver cells defines the transition from adaptive to adverse responses," *Toxicol In Vitro*, 2022.

[18] A.-M. Zavitsanou, R. Pillai, Y. Hao, et al., "KEAP1 mutation in lung adenocarcinoma promotes immune evasion and immunotherapy resistance," *Cell Rep*, vol. 42, p. 113295, 2023.

[19] M. Izumi, H. Suzumura, et al., "Differences in molecular epidemiology of lung cancer among ethnicities (Asian vs. Caucasian)," *J Thorac Dis*, vol. 12, 2020. PMID: 32802457.

[20] S. H. Park, et al., "Resistance to gefitinib and cross-resistance to irreversible EGFR-TKIs mediated by disruption of the Keap1-Nrf2 pathway in human lung cancer cells," *FASEB J*, vol. 32, no. 11, pp. 5862-5873, 2018.

[21] L. Xu, et al., "piRNA-23210 protects against acetaminophen-induced liver injury by targeting HNF1A and HNF4A," *Biochem Pharmacol*, vol. 194, p. 114897, 2021.

[22] X. Yin, et al., "Hepatotoxicity and potential mechanism of gefitinib based on CYP450 in mice and AML12 cells," *J Pharm Pharmacol*, 2023. doi:10.1093/jpp/rgac091.

[23] Y. Zhang, et al., "Mechanism of hepatotoxicity of first-line tyrosine kinase inhibitors: gefitinib and afatinib," *Toxicol Lett*, vol. 343, pp. 1-10, 2021.

[24] P. Luo, et al., "PLK1-dependent autophagy facilitates gefitinib-induced hepatotoxicity by degrading COX6A1," *Autophagy*, vol. 17, 2020.

[25] E. Krajnc, M. Visentin, Z. Gai, et al., "Untargeted metabolomics reveals anaerobic glycolysis as a novel target of the hepatotoxic antidepressant nefazodone," *J Pharmacol Exp Ther*, vol. 375, no. 2, pp. 239-246, 2020.